Striatal neuron excitability is regulated by huntingtin in the adult brain

Jessica C. Barron[1], Meghan L. Greenland[1], Fatemeh Ashrafganjoie[1], Samantha J. Carew[1], Firoozeh Nafar[1], Craig S. Moore[1] and Matthew P. Parsons[1*]

[1]Division of Biomedical Sciences, Faculty of Medicine, Memorial University of Newfoundland, St. John's, NL, Canada

*Correspondence: matthew.parsons@mun.ca

Abstract

Huntington's disease (HD) is a hereditary neurodegenerative disease that typically presents during midlife and is characterized by a combination of motor, cognitive and psychiatric symptoms. HD is fatal and arises from a mutation in the huntingtin (*HTT*) gene, which results in decreased neuronal health followed by brain atrophy, with spiny projection neurons (SPNs) of the striatum being especially vulnerable to degeneration. HTT loss-of-function, caused by haploinsufficiency of the wild type HTT gene (wt*HTT*), is an important feature of HD pathophysiology that has previously been understudied compared to mutant HTT gain-of-function mechanisms. wtHTT is essential for nervous system development and functions as a scaffolding protein to support many vital cellular functions including axonal transport, autophagy and synaptic plasticity. Here, we examined the consequences of wtHTT deletion in the adult striatum by conditionally inactivating wtHTT in 2-4 month old male and female *Htt*$^{fl/fl}$ mice. wtHTT loss of function in mature SPNs decreased intrinsic neuronal excitability and produced a neuroinflammatory response in these mice, while tissue organization, spine morphology and motor behaviour remained unaffected. Results presented here provide additional evidence that wtHTT is vital for maintaining neuronal health in the adult brain and highlight some potential adverse consequences of non-selective HTT-lowering for the treatment of HD.

47 **Introduction**

48 Huntington's disease (HD) is a monogenic neurodegenerative disease caused by an expansion of
49 35 or more CAG repeats in the huntingtin (*HTT*) gene, which leads to the production of a pathogenic
50 mutant HTT protein, and has an estimated prevalence of 13.7 per 100,000 in the general population (Fisher
51 and Hayden, 2014). Individuals with HD experience a triad of motor, cognitive and behavioural
52 symptoms, which typically present during middle age; however, symptom onset can vary from childhood
53 to late adulthood (Walker, 2007). Despite many ongoing clinical trials, there is currently no cure for this
54 fatal disease (Tabrizi et al., 2022). HD results in widespread atrophy throughout the brain, with spiny
55 projection neurons (SPNs) of the striatum being particularly vulnerable (Vonsattel et al., 1985; G.
56 Vonsattel and DiFiglia, 1998). In line with human pathology, HD mouse models recapitulate SPN-specific
57 neurodegeneration (Hodgson et al., 1999; Slow, 2003; Heikkinen et al., 2012). Whole-cell recordings from
58 HD SPNs display alterations in excitatory activity early in the disease course (Li et al., 2004; Milnerwood
59 et al., 2010, 2012). By DIV 21, SPNs co-cultured with cortical neurons from the YAC128 HD mouse
60 model have reduced dendritic arborization, fewer excitatory events and fewer readily releasable pool
61 synaptic vesicles (Buren et al., 2016). *Ex vivo*, many HD mouse models display similar alterations in SPN
62 electrophysiological properties, such as fewer sEPSC and greater spontaneous IPSC events (Cummings
63 et al., 2010). Comparable results are also seen in whole-cell recordings from striatal slices of Q175 knock-
64 in HD mice (Indersmitten et al., 2015), highlighting these electrophysiological changes as a feature of HD
65 brain pathology.

66 While mutation of the HTT protein has profound gain-of-function pathogenic effects on striatal
67 neurons, loss-of-function of wild type HTT (wtHTT) has also been shown to influence SPN health. For
68 instance, striatal neurons do not produce the essential neurotrophin, BDNF, and therefore rely on its
69 transport from the cortical projection neurons (Altar et al., 1997). wtHTT loss of function has been shown

70 to downregulate transcription of BDNF as well as disrupt its anterograde and retrograde axonal transport
71 (Zuccato et al., 2001, 2003; Gauthier et al., 2004; Colin et al., 2008; Her and Goldstein, 2008). Non-
72 pathogenic HTT is also known to have an antiapoptotic effect in HD culture and mouse models (Leavitt
73 et al., 2001, 2006). Further, previous research has shown that deletion of wtHTT in YAC128 mice
74 worsened striatal atrophy, exacerbated motor deficits and reduced survival rates (Van Raamsdonk et al.,
75 2005a). Although overexpression of wtHTT reduced striatal atrophy, this did not translate to a complete
76 rescue of motor deficits in YAC128 animals (Van Raamsdonk et al., 2006). We have previously reviewed
77 the extensive literature that supports a major role for wtHTT at the synapse (Barron et al., 2021). Notably,
78 deletion of wtHTT disrupts corticostriatal excitatory synapse development where wtHTT-depleted
79 neuronal networks were initially hyperexcitable at postnatal day 21, followed by a reduction in excitatory
80 synapse activity and density, spine maturity and dendritic complexity by 5 weeks of age (McKinstry et
81 al., 2014). wtHTT is also a critical regulator of presynaptic neurotransmission in the striatum, as its
82 deletion in striatal cultures disrupts synaptic vesicle endocytosis (McAdam et al., 2020). Other groups
83 have investigated the embryonic deletion of wtHTT in distinct subpopulations of striatal neurons, such as
84 in D1 and D2-expressing SPNs, and found it negatively impacted DARPP-32 levels and motor behaviour
85 (Mehler et al., 2019; Burrus et al., 2020). These studies provide compelling evidence for wtHTT as a
86 necessary regulator of SPN survival in the HD brain.

87 Conditional deletion of wtHTT in the dorsal hippocampus of 2-4 month *Htt*$^{fl/fl}$ mice results in
88 profound morphological deficits and widespread reactive gliosis within two months (Barron et al., 2025).
89 wtHTT-depleted CA1 pyramidal neurons also had reduced intrinsic excitability, increased spontaneous
90 EPSCs and loss of NMDAR-dependent long term potentiation (LTP) accompanied by impaired spatial
91 memory (Barron et al., 2025). These findings uncovered a novel role for wtHTT as an essential regulator
92 of hippocampal synaptic plasticity and survival. As the striatum is a particularly susceptible brain area in

93 HD and striatal neurons are known to be negatively impacted when wtHTT is deleted embryonically, we
94 hypothesized that wtHTT deletion in adult striatal SPNs would negatively impact neuronal function and
95 lead to neuroinflammation. Here, the Cre-lox system was used to inactivate *HTT* in striatal neurons of 2-
96 4 month old male and female *Htt*$^{fl/fl}$ mice. wtHTT conditional knockout (cKO) lead to significant
97 astrogliosis and decreased intrinsic neuronal excitability in these mice, implicating wtHTT as an important
98 regulator of SPN health in the adult mammalian brain.
99

100 **Materials & Methods**

101 *Animals*

102 wtHTT cKO mice were initially provided by Dr. Scott Zeitlin, University of Virginia,
103 Charlottesville, VA (Dragatsis et al., 2000). Breeding colonies were established and maintained at [Author
104 University] Animal Care facility. Mice used in these experiments have their endogenous *wtHtt* alleles
105 flanked with loxP sites to conditionally inactivate the mouse *Htt* gene in a homozygous manner by Cre
106 expression (*Htt*$^{fl/fl}$). Mice were bred as homozygous x homozygous. Equal numbers of male and female
107 mice were used for all experiments. Mice were group housed in ventilated cage racks and kept on a 12 h
108 light/dark cycle (lights on at 7:00 A.M.) with food and water available *ad libitum*. All animal procedures
109 were performed in accordance with the [Author University] animal care committee's regulations.
110

111 *Western blotting*

112 For Western blot experiments, the dorsal striatum of AAV-Cre-eGFP or AAV-eGFP-injected
113 *Htt*$^{fl/fl}$ mice were dissected and homogenized in 400 µl of lysis buffer containing halt protease and
114 phosphatase inhibitor cocktails (Thermofisher Scientific, catalog #78440). The supernatant was collected,
115 and the protein concentration was determined using bicinchoninic acid standards (Pierce Bicinchoninic

116 Acid Protein Assay Kit, Thermofisher Scientific, catalog #23227). Protein samples were prepared by
117 adding 4× lithium dodecyl sulfate sample buffer (Invitrogen, catalog # B0007) and heating at 70°C for 10
118 minutes. Samples were loaded onto a 4–12% Bis-Tris Plus gel (Invitrogen, catalog #NW04122BOX) for
119 electrophoresis. Following electrophoresis, proteins were transferred onto a 0.45 um nitrocellulose
120 membrane (Santa Cruz Biotechnology, catalog #sc-201706) using wet transfer at 24 V for 16 hours at
121 4°C. Transfer buffer contained 10% methanol. After transfer, the membrane was blocked with 5% non-
122 fat milk in Tris-buffered saline with 0.05% Tween-20 for 1 hour at room temperature to prevent
123 nonspecific binding. Primary antibodies for anti-HTT (1:1000; mouse, Sigma Aldrich, catalog
124 #MAB2166) and anti-beta-actin (1:5000, mouse, Sigma Aldrich, catalog #A5316 clone AC74), and a goat
125 anti-mouse IgG secondary antibody (1:5000, Thermofisher Scientific, catalog #31430) were used. Blots
126 were developed using a chemiluminescent horseradish peroxidase substrate (Super Signal West Pico Plus,
127 Thermofisher Scientific, catalog #34580). Band densities were quantified in FIJI (Schindelin et al., 2012),
128 and HTT band densities were normalized to actin.
129
130 *Stereotaxic surgery*
131 *Htt*$^{fl/fl}$ mice aged 2-4 months were anesthetized using isoflurane (3% induction, 1.5–2%
132 maintenance) and received a single subcutaneous injection of 2 mg/kg meloxicam in the abdomen and a
133 single 0.1 ml/0.2% lidocaine injection below the scalp. Two small holes were drilled in the skull at the
134 target brain coordinates using an Ideal Micro-Drill (Harvard Apparatus). A Model 7002 KH Neuros
135 Hamilton Syringe and an infusion pump (Pump 11 Elite Nanomite, Harvard Apparatus) were used to inject
136 1 µl pENN.AAV.hSyn.HI.eGFP-Cre.WPRE.SV40 (Addgene, catalog #105540-AAV1) or 1 µl pAAV-
137 hSyn-EGFP (Addgene, catalog #50465-AAV1) bilaterally into the dorsal striatum (injection rate, 2 nl/s).
138 The following coordinates were used with respect to distance from bregma: 0.6 mm anterior, 1.8 mm

139 medial/lateral and 2.7 mm ventral to the brain surface. The syringe was left in place for at least 5 min
140 before slow removal from the brain. Mice received a single 0.5 ml of 0.9% saline injection subcutaneously
141 in the abdominal region, and the scalp incision was sutured. Mice recovered for 20-30 minutes post-
142 surgery on a heating pad before being returned to their home cages. All experiments were performed 1-2
143 months following stereotaxic surgery.
144
145 *Acute slice preparation*
146 Mice were anesthetized using isoflurane before decapitation and whole-brain removal. Brains were
147 immersed in ice-cold oxygenated (95% O_2/5% CO_2) NMDG-HEPES artificial CSF slicing solution
148 consisting of (in mM): 92 NMDG, 2.5 KCl, 1.25 NaH_2PO_4, 30 $NaHCO_3$, 20 HEPES, 25 glucose, 2
149 thiourea, 5 Na-ascorbate, 3 Na-pyruvate, 0.5 $CaCl_2 \cdot 2H_2O$, and 10 $MgSO_4 \cdot 7H_2O$. NMDG solution was
150 adjusted with HCl to reach a pH of 7.3–7.4. Dorsal striatal acute slices from one hemisphere (the opposite
151 hemisphere was used for Golgi staining described below) were sectioned using a Precisionary
152 compresstome. Slices were then transferred into warmed (32–34 °C) NMDG-HEPES artificial CSF and
153 underwent a sodium spike-in protocol (Ting et al., 2018). After this, slices recovered for 30-45 minutes in
154 HEPES holding solution consisting of (in mM): 92 NaCl, 2.5 KCl, 1.25 NaH_2PO_4, 30 $NaHCO_3$, 20
155 HEPES, 25 glucose, 2 thiourea, 5 Na-ascorbate, 3 Na-pyruvate, 2 $CaCl_2 \cdot 2H_2O$, and 2 $MgSO_4 \cdot 7H_2O$.
156 HEPES artificial CSF solution was adjusted with NaOH to reach a pH of 7.3–7.4. Artificial CSF used
157 during electrophysiological recordings consisted of (in mM) 125 NaCl, 2.5 KCI, 25 $NaHCO_3$, 1.25
158 NaH_2PO_4, 1 $MgCl_2$, 2 $CaCl_2$, 10 glucose, and osmolarity adjusted to be approximately 310 mOsm.
159
160 *Whole-cell patch clamp electrophysiology*

161 Whole-cell patch clamp recordings of green fluorescent protein (GFP)-positive striatal neurons
162 were performed using 3-7 MΩ patch pipettes filled with potassium-gluconate internal recording solution
163 made up of (in mM) 123 potassium-gluconate, 2 $MgCl_2$, 1 KCl, 0.2 EGTA, 10 HEPES, 5 Na_2ATP, 0.3
164 Na_2GTP, with osmolarity adjusted to 285 mOsm and containing Alexa Fluor 594 Hydrazide
165 (ThermoFisher, catalog #A10442) to visualize successfully patched neurons. Only GFP-expressing
166 neurons were patched. Input-output curves were obtained in current clamp mode, injecting current from -
167 250 pA to + 400 pA in 50 pA increments. Next, cells were held in voltage clamp (Vhold = -70 mV), and
168 two minutes of stable recording was obtained to analyze sEPSC frequency and amplitude. Whole-cell
169 recordings were analyzed using ClampFit version 10.6. Detected sEPSCs with amplitudes less than 5 pA
170 were removed from the data analysis.
171
172 *Golgi staining*
173 Golgi staining was performed using Bioenno Lifesciences *sliceGolgi Kit* (catalog #003760)
174 materials and protocol. Mouse hemibrains dissected during striatal acute slice preparation described above
175 and were then submerged in a fixative buffer containing formaldehyde and glutaraldehyde. Brains
176 remained in fixative solution at 4 °C overnight. Fixed brain tissue was then coronally sectioned using a
177 Precisionary compresstome into 100 µm slices. Free-floating slices were incubated in Golgi impregnation
178 solution for 7 days in the dark at room temperature. Slices were washed one week later with 0.01 M PBS-
179 T and incubated in the remaining *sliceGolgi Kit* solutions. Striatal slices were next mounted onto gelatin-
180 coated slides, allowed to dry completely, then dehydrated in graded ethanols, cleared using xylene and
181 coverslipped with Permount mounting medium (Thermo Fisher Scientific, catalog #SP15-500). Golgi-
182 stained dendrites from striatal neurons were imaged using an Axio Observer Z1 (Zeiss) microscope with
183 a 63x/1.4NA oil-immersion objective (Zeiss). Image analysis was conducted using FIJI (Image J), where

184 spine lengths and head widths were manually traced, and their measurements were quantified. Spine
185 morphology was categorized using the following parameters: length less than 1 µm = stubby spine; length
186 greater than 1 µm and width less than 0.5 µm = thin spine; length greater than 1 µm and width greater
187 than 0.5 µm = mushroom spine (Risher et al., 2014).
188
189 *Histological Staining*
190 Mice were perfused intracardially using 4% paraformaldehyde to achieve fixation, and whole
191 brains were dissected. Mice were held under anathesia during the fixation procedure by the use of
192 isoflurane (3% induction, maintained at 5% during perfusion). Fixed brains remained in 4%
193 paraformaldehyde for one week and then briefly in 10% normal buffered formalin. Brains were then
194 dehydrated starting with 70% ethanol, followed by 80%, 95% and absolute ethanol, followed by 100%
195 xylene before paraffin embedding. Paraffin-embedded brain tissue was then processed into 8µm coronal
196 sections using an automated vacuum infiltration tissue processor (TissueTek V.I.P. 5, Sakura Finetek
197 USA). For the H&E protocol, slides were dipped in two changes of xylene for 5 minutes each. They were
198 then re-hydrated, starting with absolute ethanol, followed by 95%, 80%, and 70% ethanol and then washed
199 with tap water for 2 minutes. Following rehydration, slides were stained with Mayer's hematoxylin
200 solution (Millipore Sigma, catalog #109249) for 10-15 minutes and rinsed with tap water for 2 minutes.
201 Slides were placed in Scott's tap water substitute for 2 minutes and washed with tap water for 5 minutes.
202 Next, slides were counterstained in eosin for 15 seconds to 2 minutes. Slides were then dehydrated with
203 95% ethanol twice for 30 seconds each, followed by 30 seconds in absolute ethanol. Slides were cleared
204 in 3 changes of xylene, 1 minute each, and mounted with xylene-based mounting medium and
205 coverslipped. Nuclei were stained blue, and cytoplasmic compartments were stained various shades of
206 pink, which were used to identify tissue components. For the cresyl violet staining protocol, sections were

207 deparaffinized and re-hydrated as described above. Slides were then stained with cresyl violet stain
208 solution (1%) (Abcam, catalog #ab246817) for 3-5 minutes and rinsed with distilled water. Slides were
209 then dehydrated with absolute ethanol, cleared with xylene, mounted and coverslipped as above. Nissl
210 substance was stained violet, which was used to identify neuronal cell bodies. Images of H&E and cresyl
211 violet stained slides were taken using an EVOS M5000 microscope (Thermo Fisher Scientific) with a
212 20x/0.8NA objective (Olympus). Neuropathology based on these histology stains was qualitatively
213 assessed by a blind reviewer.
214
215 *Immunohistochemistry*
216 A IHC hydrophobic barrier was drawn around striatal slides using a DAKO Pen (Agilent
217 Technologies, catalog #s200230-2) which were then washed briefly in 1xPBS solution. Striatal slides were
218 then submerged in a blocking solution consisting of 5% bovine serum albumin and 0.2% Triton-X in
219 1xPBS for 1 hour at room temperature. After blocking, primary antibodies (chicken anti-GFP, 1:500,
220 Abcam, catalog #ab13970; mouse anti-GFAP, 1:500, Millipore Sigma, catalog #MAB3402; rabbit anti-
221 IBA-1, 1:500, Cedarlane, catalog #019-19741) were diluted in a 1% bovine serum albumin/0.2% Triton-
222 X PBS solution and incubated overnight on at 4 °C. On the second day, slides were washed with 1xPBS
223 and secondary antibodies (Alexa Fluor 488, goat anti-chicken, 1:500, Invitrogen, catalog #A-11039; Alexa
224 Fluor 594, goat anti-rabbit, 1:500, Invitrogen, catalog #A-11037; Alexa Fluor 647, goat anti-mouse, 1:500,
225 Invitrogen, catalog #A11029) diluted in a 1% bovine serum albumin/0.2% Triton-X PBS solution and
226 incubated in the dark for 2 hours at room temperature. Slides were then washed with 1xPBS and
227 coverslipped with DAPI Fluoroshield mounting medium to visualize nuclei (Abcam, catalog #ab104139).
228 All images were taken using either a Axio Observer Z1 (Zeiss) microscope with a 20x/0.8NA objective
229 (Zeiss) or a EVOS M5000 (Thermo Fisher Scientific) microscope with a 20x/0.8NA objective (Olympus).

230 Consistent imaging settings were used within each experiment. For GFAP and IBA-1 analysis, percent
231 positive area values were quantified by applying a constant threshold value to all images. Percent positive
232 area and mean gray (intensity) values were calculated using FIJI (Schindelin et al., 2012).
233
234 *Behaviour*
235 *Open field test (OFT)*
236 All testing was done between 8:00 A.M. and 5 P.M. In all behavioural tests described, testing times
237 were counterbalanced among groups. All equipment was washed with 70% ethanol following each test.
238 For OFT, mice were videotaped during a 10-minute exploration of a brightly lit open field within a 50 cm
239 × 50 cm white Plexiglass box. Distance travelled and mean velocity were scored using ANYMaze
240 software (Wood Dale, IL, USA). Animals with <2 cm/s mean velocity were excluded from analysis for
241 failing to explore the arena. Trials in which ANYMaze failed to track the animal more than 10% of the
242 time were excluded from analysis.
243
244 *Accelerated Rotarod*
245 Mice learned to run when placed on a rotating rod (rotarod) that accelerated from 4 to 40 rotations
246 per minute for 300 seconds. When they fell, the experimenter stopped the rotarod manually. For some
247 trials, the mice rotated around the rotarod instead of falling, which was considered equivalent to a fall.
248 Mice performed three trials/day for 4 days with a 1.5- to 2-hour intertrial interval. Latency to fall, number
249 of rotations (around the rod) and number of turn arounds (where the mouse faces backwards) were
250 recorded.
251
252 *Statistics*

253 All statistical tests were performed using version 10.2.2 GraphPad Prism. Animal number (N) and
254 cell/image/slice number (n) values, specific statistical tests used, p values, F values and degrees of freedom
255 are described in Table 1. Outliers were identified using the ROUT method (Q = 1%). P values less than
256 0.05 were considered significant.
257
258 **Results**
259 *Experimental design and validation of huntingtin conditional knockout in the striatum*
260 To investigate the consequences of wtHTT knockout in adult striatal neurons, synapsin-promoted
261 AAV-eGFP-Cre or AAV-eGFP was injected into the dorsal striatum of 2–4-month-old male and female
262 *Htt*$^{fl/fl}$ mice. All experiments took place 1-2 months post-injection and brains were assessed using
263 histological, immunohistochemical electrophysiological and behavioural methods (Fig. 1A). Viral
264 targeting was confirmed by IHC, where GFP was expressed widely throughout the mouse dorsal striatum,
265 indicating the injection delivery strategy was successful (Fig. 1B). cKO of the wtHTT protein was
266 validated by Western blot methods where Cre-injected animals had a 43.6% reduction in HTT levels on
267 average from total brain tissue lysate 1-2 months post-surgery (Fig. 1C, p = 0.0061). A complete depletion
268 of HTT was not expected in these total protein samples, as the tissue samples used included many non-
269 neuronal cells that would still express normal levels of HTT. These results indicated that wtHTT levels
270 were successfully depleted in the dorsal striatum of these animal models.
271
272 *Huntingtin knockout does not impact general morphology in the adult striatum but leads to astrogliosis*
273 We first wanted to determine how deletion of the wtHTT protein in adulthood would affect the
274 general morphology of the striatum, as it was previously found that 1-2 months of wtHTT deletion in the
275 adult mouse hippocampus had profound adverse effects on CA1 tissue organization (Barron et al., 2025).

276 Here, control and cKO H&E-stained slides were qualitatively assessed for changes in tissue organization
277 and cell density, as well as for signs of inflammation or neurodegeneration. No obvious signs of
278 neuropathology could be detected with either H&E staining (Fig. 2A) or cresyl violet staining (Fig. 2B).
279 Next, total cell density was investigated using nuclear marker DAPI to assess if wtHTT deletion impacted
280 cell counts. These experiments showed that wtHTT cKO had only a non-significant trend towards
281 increased nuclear density in the dorsal striatum (Fig. 2D, $p = 0.0865$). Spine density and morphology was
282 also assessed by Golgi methods (Fig. 2C). Based on the Golgi experiments, no observable differences
283 were seen between spine morphology of control and wtHTT knockout striatal neurons (Fig. 2C, spine
284 density $p = 0.458$, thin spines $p = 0.186$, stubby spines $p = 0.613$, mushroom spines $p = 0.382$). Overall,
285 1-2 months wtHTT reduction did not impact tissue morphology or spine dynamics in the adult mouse
286 brain.

287 The HD striatum is marked by significant gliosis, which correlates with disease progression
288 (Vonsattel et al., 1985). Here, 1-2 month wtHTT cKO in striatal neurons also resulted in increased GFAP
289 intensity (Fig. 3A; Fig 3B, $p = 0.0085$) and a trend towards increased GFAP percent positive area (Fig.
290 3D, $p = 0.0750$). However, quantification of IBA-1 immunostaining did not yield any significant
291 differences in overall intensity or percent positive area values (Fig. 3C, $p = 0.658$; Fig. 3E, $p = 0.235$).
292 Results here show that 1-2 month wtHTT knockout in the dorsal striatum leads to reactive astrogliosis,
293 while microglia levels remain unchanged in these animals.

294

295 *Deletion of huntingtin decreases intrinsic excitability in the mouse striatum*

296 Next, whole-cell patch clamping was used to investigate changes in cell excitability after wtHTT
297 cKO in striatal neurons. wtHTT deletion in the striatum resulted in extensive changes in intrinsic cell
298 properties (Fig. 4A-G). wtHTT cKO neurons fired much fewer action potentials (APs) compared to their

299 control GFP counterparts (Fig. 4B, p = 0.0003), which was accompanied by an increased rheobase (Fig.
300 4C, p = 0.0001) and AP threshold (Fig. 4D p = 0.0002), indicating more positive current was required to
301 elicit an AP. Other basic neuronal properties were impacted by wtHTT loss, including a hyperpolarized
302 resting membrane potential (RMP) (Fig. 4E, p = 0.0192) and a decrease in membrane resistance (Fig. 4F,
303 p = 0.0056), while membrane capacitance remained unchanged, suggesting no changes in cell size (Fig.
304 4G, p = 0.5264). Changes in sEPSCs in striatal neurons were also assessed after wtHTT loss. Data from
305 these recordings show that the average frequency of spontaneous events and interevent interval (IEI)
306 values were unchanged after wtHTT loss of function (Fig. 4I, p = 0.177; Fig. 4J, p = 0.177). However, a
307 trending increase in sEPSC amplitude was observed (Fig. 4K, p = 0.0585). In sum, wtHTT deletion in the
308 adult striatum resulted in profound changes in intrinsic cell excitability, while excitatory
309 neurotransmission remained generally unaffected.
310
311 *1-2 month huntingtin knockout in the mouse striatum does not influence general motor activity or motor*
312 *learning*
313 Lastly, we assessed the impact of wtHTT deletion on motor function. To do this, overall motor
314 activity of control and cKO mice was quantified using an open field test (OFT) paradigm where mice were
315 tracked using ANYmaze software (Fig. 5A). The same datasets but separated by sex can be viewed in
316 supplementary data (Fig. S1). Average total distance and average speed during the ten-minute testing trial
317 were found to be comparable between control and wtHTT cKO mice, indicating that HTT depletion in
318 striatal neurons did not impact general motor activity in these animals (Fig. 5B, p = 0.512; Fig 5C, p =
319 0.5244). Next, mice were trained to run on an accelerating rotarod. This behavioural test is commonly
320 used to quantify motor skill learning, and HD mice have significant impairments in rotarod motor learning
321 (Van Raamsdonk et al., 2005b). For these experiments, mice were trained three times a day for 4 days,

322 and latency to fall during each session was recorded. Both wtHTT cKO and control animals learned this
323 behavioural test, with females performing statistically better overall compared to males (Fig. S1B, $p =$
324 0.0062). However, no differences were seen in average latency to fall over the training sessions (Fig. 5C,
325 $p = 0.888$). In all, these data show that motor behaviour was comparable between control and striatal cKO
326 animals.
327
328 **Discussion**
329 Results presented here demonstrate that wtHTT deletion in adult MSNs leads to reactive gliosis
330 and decreased intrinsic neuronal excitability, while tissue morphology, spine dynamics and cell density in
331 the striatum remain unchanged after 1-2 months wtHTT loss of function. Additionally, no differences in
332 general motor activity or motor learning were observed after conditional wtHTT deletion in these animals.
333 Although previous HTT-lowering studies have reported that wtHTT deletion is well tolerated in the non-
334 human primate brain (McBride et al., 2011; Grondin et al., 2012), significant inflammatory and
335 electrophysiological changes were discerned in these conditional knockout mouse models that may have
336 been overlooked in previous studies evaluating the role of wtHTT in the striatum.
337
338 *Huntingtin deletion in the dorsal striatum does not impact brain morphology*
339 Striatal neurodegeneration is a pathological hallmark of HD. The caudate and putamen structures
340 that together make up the striatum of the basal ganglia undergo extensive volume loss, mainly due to the
341 death of GABAergic SPNs, which comprise roughly 95% of neurons in this brain region (Vonsattel et al.,
342 1985; G. Vonsattel and DiFiglia, 1998). Paradoxically, although HTT is ubiquitously expressed
343 throughout the brain, striatal neurons have surprisingly low levels of HTT in health and disease states
344 compared to other brain areas, such as the cortex and the CA2/CA3 hippocampus (Reiner et al., 2003).

345 Striatal SPNs are especially vulnerable to the expression of mutant HTT, and many hypotheses regarding
346 this distinct susceptibility have been reviewed elsewhere (Han et al., 2010). One prominent theory is that
347 SPNs are discordantly impacted by transcriptional dysregulation in HD and undergo significant loss of
348 cell type identity (Malaiya et al., 2021; Obenauer et al., 2022; Matsushima et al., 2023). Based on their
349 unique susceptibility to cell death in HD, it was anticipated that wtHTT deletion would lead to atrophy
350 that would be detectable at the tissue level. Surprisingly, wtHTT-deficient striatal neurons in this model
351 showed no differences in qualitative analysis of tissue morphology and quantitative analysis of nuclear
352 density compared to controls. Similar studies have also reported that striatal morphology is unchanged
353 after tamoxifen-induced wtHTT-lowering in wild-type mice (Dietrich et al., 2017). Transcriptional
354 dysregulation in the HD striatum may, therefore, be driven by a gain-of-function mechanism as opposed
355 to wtHTT loss-of-function. Regio *et al.* recently found that when wtHTT was deleted by Cas9 gene editing
356 in adult wild-type FVB mice, transcriptional profiles of these animals were comparable to controls (Regio
357 et al., 2023). Striatal brain morphology was also normal in these animals, similar to what was observed
358 here (Regio et al., 2023). We have previously shown that wtHTT reduction in primary hippocampal
359 neurons results in a loss of transcriptional repression and altered chromatin morphology (Barron et al.,
360 unpublished observations). Still, perhaps these effects differ regionally between the hippocampus and
361 striatum in adulthood. It will be of interest for future studies to investigate the implications of wtHTT
362 reduction in the context of transcriptional dysregulation in the adult hippocampus.
363
364 *Reactive astrogliosis but not microgliosis in the dorsal striatum after 1-2 month huntingtin knockout*
365 Starting early in the HD disease course, there is an increase in intensity levels of GFAP and IBA-
366 1, astrocyte and microglia markers, respectively, and these glial cell types exhibit morphology deficits
367 (Dowie et al., 2014). In line with this, HD patients and mouse models also display elevated levels of

368 inflammatory cytokines and chemokines (Björkqvist et al., 2008; Wild et al., 2011). wtHTT loss of
369 function has been previously implicated in HD neuroinflammation. For instance, wtHTT-lowered human-
370 derived macrophages are functionally impaired and are more vulnerable to stress (O'Regan et al., 2020).
371 Additionally, (Dietrich et al., 2017) have shown that 9 months of global wtHTT deletion in adulthood
372 results in extensive astrogliosis. Here, 1-2 months of wtHTT cKO was sufficient to elicit widespread
373 astrocyte reactivity in the mouse striatum. However, although it was previously found that wtHTT deletion
374 in the hippocampus increased IBA-1 presence (Barron et al., 2025), no changes in microglial levels were
375 detected in the current study. It is possible that the onset of microgliosis was simply missed given that
376 microglia are one of the first immune cell types to respond to injury in the brain, with astrocytes becoming
377 active much later (Fawcett and Asher, 1999). Astrocytes form close associations with neurons to create
378 tripartite synapses and are important regulators of synaptic neurotransmission (Araque et al., 1999). It was
379 recently proposed that astrocytes may also regulate intrinsic excitability of neurons, as activation of
380 hippocampal astrocytes led to a decrease in neuronal intrinsic excitation through adenosine signalling
381 (Expósito et al., 2024). This could be a possible mechanism underlying the change in neuronal excitability
382 seen in both HTT conditional knockout mouse models.
383
384 *Huntingtin deletion reduces intrinsic excitability of adult striatal neurons*
385 wtHTT cKO in the adult mouse striatum resulted in a major deficit in intrinsic excitation. Striatal
386 SPNs receive extensive excitatory inputs from neighbouring brain areas, mainly in the form of
387 glutamatergic signalling from the cortex and thalamus and dopaminergic signalling from the ventral
388 tegmental area and substantia nigra pars compacta (Nelson and Kreitzer, 2014). These neurons then project
389 through direct pathway SPNs or indirect pathway SPNs to regulate voluntary and involuntary movement,
390 respectively. Experiments used herein did not differentiate between direct and indirect pathway SPNs.

391 However, embryonic wtHTT deletion in either of these neuronal subsets has been previously shown to
392 impact the inhibitory activity of globus pallidus neurons (Burrus et al., 2020). The decrease in SPN firing
393 seen here could partly explain the change in inhibitory activity previously seen within these synaptic
394 targets in the globus pallidus. Dorsal striatal neurons express both AMPARs and NMDARs to receive
395 glutamatergic input from the cortex and thalamus (Jeun et al., 2009). wtHTT is known to influence
396 AMPAR responses, likely by promoting their transport to the synapse (Mandal et al., 2011; Wennagel et
397 al., 2022). Non-pathogenic HTT may also impact the trafficking of NMDARs through its association with
398 HIP14 and HIP14-like proteins (Huang et al., 2011). Although sEPSC events from control and wtHTT
399 cKO striatal neurons were statistically comparable, a trending increase in sEPSC amplitude was noted (p
400 $= 0.0585$), indicating that AMPAR levels may be altered. Given that direct and indirect pathway SPNs are
401 distinct in their postsynaptic receptor expression, downstream effects on motor activity, and pathogenesis
402 in HD, it is possible that changes in spontaneous excitatory activity differed between these striatal cell
403 types. Therefore, the present study may have been unable to detect these cell type-specific changes
404 (Kravitz et al., 2010; Oldenburg and Sabatini, 2015; Lee et al., 2016; Barry et al., 2018). The impact of
405 wtHTT loss in adulthood on striatal excitation remains an important area of investigation, given the critical
406 role of the striatum in basal ganglia synaptic circuitry and HD. Although changes in motor activity were
407 not observed in these experiments, previous studies investigating this have yielded mixed results. Global
408 deletion of wtHTT between 3-9 months in mice elicited progressive motor deficits, including decreased
409 latency to fall from an accelerated rotarod (Dietrich et al., 2017). While wtHTT knockout more specifically
410 targeted to the adult striatum and projecting areas showed no behavioural deficits in a comprehensive
411 motor assessment (Regio et al., 2023). Therefore, the previously identified effects on motor performance
412 may be due to wtHTT-lowering in another brain area downstream from the striatum, such as the cortex.

413 Overall, wtHTT conditional deletion in adult striatal SPNs decreased intrinsic neuronal excitability
414 and produced an astrogliosis response, while tissue organization, spine morphology, cell density and
415 motor phenotypes remained unaffected. Results presented here contribute additional evidence to the
416 growing body of literature that demonstrate wtHTT loss of function negatively impacts neuronal health in
417 the adult brain and caution that substantial reduction of wtHTT levels through the use of non-selective
418 HTT-lowering therapeutics may have adverse molecular consequences such as those identified here.
419

420 **Acknowledgements:** We would like to thank Dr. Scott Zeitlin (University of Virginia) for providing us
421 with our initial $Htt^{fl/fl}$ mouse colonies that were bred and used for all experiments. We would also like to
422 thank the Animal Care Services staff at Memorial University for their assistance with the housing,
423 monitoring and care of all research animals used for these experiments. All research presented in the
424 current manuscript was funded by Dr. Parsons' Canadian Institutes of Health Research (CIHR) project
425 grant.
426

427 **Author Contributions**

428 JCB and MPP designed research; JCB, MLG, EPH, FA, FN, CSM and MPP performed research; JCB
429 analyzed data; JCB wrote the paper with feedback from MPP.
430

431 **Declaration of Interests**

432 The authors declare no competing interests.
433
434
435

436 **References**

437 Altar CA, Cai N, Bliven T, Juhasz M, Conner JM, Acheson AL, Lindsay RM, Wiegand SJ (1997)
438 Anterograde transport of brain-derived neurotrophic factor and its role in the brain. Nature
439 389:856–860.

440 Araque A, Parpura V, Sanzgiri RP, Haydon PG (1999) Tripartite synapses: glia, the unacknowledged
441 partner. Trends Neurosci 22:208–215.

442 Barron JC, Dawson LJ, Carew SJ, Grace MC, Senior KA, Ryan KC, Nafar F, Moore CS, Blundell J,
443 Parsons MP (2025) Huntingtin plays an essential role in the adult hippocampus. Neurobiol Dis
444 206:106810.

445 Barron JC, Hurley EP, Parsons MP (2021) Huntingtin and the Synapse. Front Cell Neurosci 15:689332.

446 Barry J, Akopian G, Cepeda C, Levine MS (2018) Striatal Direct and Indirect Pathway Output
447 Structures Are Differentially Altered in Mouse Models of Huntington's Disease. J Neurosci
448 38:4678–4694.

449 Björkqvist M et al. (2008) A novel pathogenic pathway of immune activation detectable before clinical
450 onset in Huntington's disease. J Exp Med 205:1869–1877.

451 Buren C, Parsons MP, Smith-Dijak A, Raymond LA (2016) Impaired development of cortico-striatal
452 synaptic connectivity in a cell culture model of Huntington's disease. Neurobiol Dis.

453 Burrus CJ, McKinstry SU, Kim N, Ozlu MI, Santoki AV, Fang FY, Ma A, Karadeniz YB, Worthington
454 AK, Dragatsis I, Zeitlin S, Yin HH, Eroglu C (2020) Striatal Projection Neurons Require
455 Huntingtin for Synaptic Connectivity and Survival. Cell Rep 30:642-657.e6.

456 Colin E, Zala D, Liot G, Rangone H, Borrell-Pagès M, Li XJ, Saudou F, Humbert S (2008) Huntingtin
457 phosphorylation acts as a molecular switch for anterograde/retrograde transport in neurons.
458 EMBO J 27:2124–2134.

459 Cummings DM, Cepeda C, Levine MS (2010) Alterations in Striatal Synaptic Transmission are
460 Consistent across Genetic Mouse Models of Huntington's Disease. ASN Neuro 2:AN20100007.
461 Dietrich P, Johnson IM, Alli S, Dragatsis I (2017) Elimination of huntingtin in the adult mouse leads to
462 progressive behavioral deficits, bilateral thalamic calcification, and altered brain iron
463 homeostasis. PLoS Genet 13:1–29.
464 Dowie MJ, Grimsey NL, Hoffman T, Faull RLM, Glass M (2014) Cannabinoid receptor CB2 is
465 expressed on vascular cells, but not astroglial cells in the post-mortem human Huntington's
466 disease brain. J Chem Neuroanat 59–60:62–71.
467 Dragatsis I, Levine MS, Zeitlin S (2000) Inactivation of Hdh in the brain and testis results in progressive
468 neurodegeneration and sterility in mice. Nat Genet.
469 Expósito S, Alberquilla S, Martín ED (2024) Astrocytes tune neuronal excitability through the Ca^{2+} -
470 activated K^{+} current sIAHP.
471 Fawcett JW, Asher RichardA (1999) The glial scar and central nervous system repair. Brain Res Bull
472 49:377–391.
473 Fisher ER, Hayden MR (2014) Multisource ascertainment of Huntington disease in Canada: Prevalence
474 and population at risk. Mov Disord 29:105–114.
475 G. Vonsattel JP, DiFiglia M (1998) Huntington Disease: J Neuropathol Exp Neurol 57:369–384.
476 Gauthier LR, Charrin BC, Borrell-Pagès M, Dompierre JP, Rangone H, Cordelières FP, De Mey J,
477 MacDonald ME, Leßmann V, Humbert S, Saudou F (2004) Huntingtin controls neurotrophic
478 support and survival of neurons by enhancing BDNF vesicular transport along microtubules. Cell
479 118:127–138.

480 Grondin R, Kaytor MD, Ai Y, Nelson PT, Thakker DR, Heisel J, Weatherspoon MR, Blum JL, Burright
481 EN, Zhang Z, Kaemmerer WF (2012) Six-month partial suppression of Huntingtin is well
482 tolerated in the adult rhesus striatum. Brain.
483 Han I, You Y, Kordower JH, Brady ST, Morfini GA (2010) Differential vulnerability of neurons in
484 Huntington's disease: the role of cell type-specific features. J Neurochem 113:1073–1091.
485 Heikkinen T, Lehtimäki K, Vartiainen N, Puoliväli J, Hendricks SJ, Glaser JR, Bradaia A, Wadel K,
486 Touller C, Kontkanen O, Yrjänheikki JM, Buisson B, Howland D, Beaumont V, Munoz-Sanjuan
487 I, Park LC (2012) Characterization of Neurophysiological and Behavioral Changes, MRI Brain
488 Volumetry and 1H MRS in zQ175 Knock-In Mouse Model of Huntington's Disease. PLoS ONE
489 7:e50717.
490 Her LS, Goldstein LSB (2008) Enhanced sensitivity of striatal neurons to axonal transport defects
491 induced by mutant huntingtin. J Neurosci 28:13662–13672.
492 Hodgson JG et al. (1999) A YAC mouse model for Huntington's disease with full-length mutant
493 huntingtin, cytoplasmic toxicity, and selective striatal neurodegeneration. Neuron.
494 Huang K, Sanders SS, Kang R, Carroll JB, Sutton L, Wan J, Singaraja R, Young FB, Liu L, El-Husseini
495 A, Davis NG, Hayden MR (2011) Wild-type HTT modulates the enzymatic activity of the
496 neuronal palmitoyl transferase HIP14. Hum Mol Genet 20:3356–3365.
497 Indersmitten T, Tran CH, Cepeda C, Levine MS (2015) Altered excitatory and inhibitory inputs to
498 striatal medium-sized spiny neurons and cortical pyramidal neurons in the Q175 mouse model of
499 Huntington's disease. J Neurophysiol 113:2953–2966.
500 Jeun SH, Cho HS, Kim KJ, Li QZ, Sung K-W (2009) Electrophysiological Characterization of AMPA
501 and NMDA Receptors in Rat Dorsal Striatum. Korean J Physiol Pharmacol 13:209.

502 Kravitz AV, Freeze BS, Parker PRL, Kay K, Thwin MT, Deisseroth K, Kreitzer AC (2010) Regulation
503 of parkinsonian motor behaviours by optogenetic control of basal ganglia circuitry. Nature
504 466:622–626.
505 Leavitt BR, Guttman JA, Hodgson JG, Kimel GH, Singaraja R, Vogl AW, Hayden MR (2001) Wild-
506 type Huntingtin reduces the cellular toxicity of mutant Huntingtin in vivo. Am J Hum Genet
507 68:313–324.
508 Leavitt BR, Van Raamsdonk JM, Shehadeh J, Fernandes H, Murphy Z, Graham RK, Wellington CL,
509 Raymond LA, Hayden MR (2006) Wild-type huntingtin protects neurons from excitotoxicity. J
510 Neurochem 96:1121–1129.
511 Lee HJ, Weitz AJ, Bernal-Casas D, Duffy BA, Choy M, Kravitz AV, Kreitzer AC, Lee JH (2016)
512 Activation of Direct and Indirect Pathway Medium Spiny Neurons Drives Distinct Brain-wide
513 Responses. Neuron 91:412–424.
514 Li L, Murphy TH, Hayden MR, Raymond LA (2004) Enhanced Striatal NR2B-Containing *N* -Methyl- D
515 -Aspartate Receptor-Mediated Synaptic Currents in a Mouse Model of Huntington Disease. J
516 Neurophysiol 92:2738–2746.
517 Malaiya S, Cortes-Gutierrez M, Herb BR, Coffey SR, Legg SRW, Cantle JP, Colantuoni C, Carroll JB,
518 Ament SA (2021) Single-Nucleus RNA-Seq Reveals Dysregulation of Striatal Cell Identity Due
519 to Huntington's Disease Mutations. J Neurosci 41:5534–5552.
520 Mandal M, Wei J, Zhong P, Cheng J, Duffney LJ, Liu W, Yuen EY, Twelvetrees AE, Li S, Li XJ,
521 Kittler JT, Yan Z (2011) Impaired α-amino-3-hydroxy-5-methyl-4-isoxazolepropionic acid
522 (AMPA) receptor trafficking and function by mutant Huntingtin. J Biol Chem 286:33719–33728.

523 Matsushima A, Pineda SS, Crittenden JR, Lee H, Galani K, Mantero J, Tombaugh G, Kellis M, Heiman
524 M, Graybiel AM (2023) Transcriptional vulnerabilities of striatal neurons in human and rodent
525 models of Huntington's disease. Nat Commun 14:282.
526 McAdam RL, Morton A, Gordon SL, Alterman JF, Khvorova A, Cousin MA, Smillie KJ (2020) Loss of
527 huntingtin function slows synaptic vesicle endocytosis in striatal neurons from the httQ140/Q140
528 mouse model of Huntington's disease. Neurobiol Dis 134:104637.
529 McBride JL, Pitzer MR, Boudreau RL, Dufour B, Hobbs T, Ojeda SR, Davidson BL (2011) Preclinical
530 safety of RNAi-mediated HTT suppression in the rhesus macaque as a potential therapy for
531 Huntington's disease. Mol Ther.
532 McKinstry SU, Karadeniz YB, Worthington AK, Hayrapetyan VY, Ozlu MI, Serafin-Molina K, Risher
533 WC, Ustunkaya T, Dragatsis I, Zeitlin S, Yin HH, Eroglu C (2014) Huntingtin Is Required for
534 Normal Excitatory Synapse Development in Cortical and Striatal Circuits. J Neurosci 34:9455–
535 9472.
536 Mehler MF, Petronglo JR, Arteaga-Bracho EE, Gulinello ME, Winchester ML, Pichamoorthy N, Young
537 SK, DeJesus CD, Ishtiaq H, Gokhan S, Molero AE (2019) Loss-of-Huntingtin in Medial and
538 Lateral Ganglionic Lineages Differentially Disrupts Regional Interneuron and Projection Neuron
539 Subtypes and Promotes Huntington's Disease-Associated Behavioral, Cellular, and Pathological
540 Hallmarks. J Neurosci 39:1892–1909.
541 Milnerwood AJ, Gladding CM, Pouladi MA, Kaufman AM, Hines RM, Boyd JD, Ko RWY, Vasuta OC,
542 Graham RK, Hayden MR, Murphy TH, Raymond LA (2010) Early Increase in Extrasynaptic
543 NMDA Receptor Signaling and Expression Contributes to Phenotype Onset in Huntington's
544 Disease Mice. Neuron.

545 Milnerwood AJ, Kaufman AM, Sepers MD, Gladding CM, Zhang L, Wang L, Fan J, Coquinco A, Qiao
546 JY, Lee H, Wang YT, Cynader M, Raymond LA (2012) Mitigation of augmented extrasynaptic
547 NMDAR signaling and apoptosis in cortico-striatal co-cultures from Huntington's disease mice.
548 Neurobiol Dis 48:40–51.
549 Nelson AB, Kreitzer AC (2014) Reassessing Models of Basal Ganglia Function and Dysfunction. Annu
550 Rev Neurosci 37:117–135.
551 Obenauer JC, Chen J, Andreeva V, Aaronson JS, Lee R, Caricasole A, Rosinski J (2022) Expression
552 analysis of Huntington disease mouse models reveals robust striatum disease signatures.
553 Oldenburg IA, Sabatini BL (2015) Antagonistic but Not Symmetric Regulation of Primary Motor Cortex
554 by Basal Ganglia Direct and Indirect Pathways. Neuron 86:1174–1181.
555 O'Regan GC, Farag SH, Ostroff GR, Tabrizi SJ, Andre R (2020) Wild-type huntingtin regulates human
556 macrophage function. Sci Rep.
557 Regio S, Vachey G, Goñi E, Duarte F, Rybarikova M, Sipion M, Rey M, Huarte M, Déglon N (2023)
558 Revisiting the outcome of adult wild-type *Htt* inactivation in the context of *HTT* -lowering
559 strategies for Huntington's disease. Brain Commun 5:fcad344.
560 Reiner A, Dragatsis I, Zeitlin S, Goldowitz D (2003) Wild-Type Huntingtin Plays a Role in Brain
561 Development and Neuronal Survival. Mol Neurobiol.
562 Risher WC, Ustunkaya T, Singh Alvarado J, Eroglu C (2014) Rapid Golgi Analysis Method for
563 Efficient and Unbiased Classification of Dendritic Spines. PLoS ONE 9:e107591.
564 Schindelin J, Arganda-Carreras I, Frise E, Kaynig V, Longair M, Pietzsch T, Preibisch S, Rueden C,
565 Saalfeld S, Schmid B, Tinevez J-Y, White DJ, Hartenstein V, Eliceiri K, Tomancak P, Cardona
566 A (2012) Fiji: an open-source platform for biological-image analysis. Nat Methods 9:676–682.

567 Slow EJ (2003) Selective striatal neuronal loss in a YAC128 mouse model of Huntington disease. Hum
568 Mol Genet 12:1555–1567.
569 Tabrizi SJ, Estevez-Fraga C, van Roon-Mom WMC, Flower MD, Scahill RI, Wild EJ, Muñoz-Sanjuan
570 I, Sampaio C, Rosser AE, Leavitt BR (2022) Potential disease-modifying therapies for
571 Huntington's disease: lessons learned and future opportunities. Lancet Neurol 21:645–658.
572 Ting JT, Lee BR, Chong P, Soler-Llavina G, Cobbs C, Koch C, Zeng H, Lein E (2018) Preparation of
573 Acute Brain Slices Using an Optimized N-Methyl-D-glucamine Protective Recovery Method. J
574 Vis Exp 53825.
575 Van Raamsdonk JM, Pearson J, Murphy Z, Hayden MR, Leavitt BR (2006) Wild-type huntingtin
576 ameliorates striatal neuronal atrophy but does not prevent other abnormalities in the YAC128
577 mouse model of Huntington disease. BMC Neurosci 7:80.
578 Van Raamsdonk JM, Pearson J, Rogers DA, Bissada N, Vogl AW, Hayden MR, Leavitt BR (2005a)
579 Loss of wild-type huntingtin influences motor dysfunction and survival in the YAC128 mouse
580 model of Huntington disease. Hum Mol Genet 14:1379–1392.
581 Van Raamsdonk JM, Pearson J, Slow EJ, Hossain SM, Leavitt BR, Hayden MR (2005b) Cognitive
582 Dysfunction Precedes Neuropathology and Motor Abnormalities in the YAC128 Mouse Model
583 of Huntington's Disease. J Neurosci 25:4169–4180.
584 Vonsattel JP, Myers RH, Stevens TJ, Ferrante RJ, Bird ED, Richardson EP (1985) Neuropathological
585 classification of huntington's disease. J Neuropathol Exp Neurol.
586 Walker FO (2007) Huntington's disease. Lancet 369:218–228.
587 Wennagel D, Braz BY, Capizzi M, Barnat M, Humbert S (2022) Huntingtin coordinates dendritic spine
588 morphology and function through cofilin-mediated control of the actin cytoskeleton. Cell Rep
589 40:111261.

590 Wild E, Magnusson A, Lahiri N, Krus U, Orth M, Tabrizi SJ, Björkqvist M (2011) Abnormal peripheral
591 chemokine profile in Huntington's disease. PLoS Curr 3:RRN1231.
592 Zuccato C, Ciammola A, Rigamonti D, Leavitt BR, Goffredo D, Conti L, MacDonald ME, Friedlander
593 RM, Silani V, Hayden MR, Timmusk T, Sipione S, Cattaneo E (2001) Loss of huntingtin-
594 mediated BDNF gene transcription in Huntington's disease. Science 293:493–498.
595 Zuccato C, Tartari M, Crotti A, Goffredo D, Valenza M, Conti L, Cataudella T, Leavitt BR, Hayden
596 MR, Timmusk T, Rigamonti D, Cattaneo E (2003) Huntingtin interacts with REST/NRSF to
597 modulate the transcription of NRSE-controlled neuronal genes. Nat Genet 35:76–83.
598
599
600
601
602
603
604
605
606
607
608
609
610
611
612

613 **Figure Legends**

614 Figure 1. Experimental design and striatal conditional knockout mouse model validation. A
615 Representative images showing AAV-eGFP expression and DAPI stained nuclei. Scale bar: 25 µm. B
616 Experimental methods and timeline. C Left: Total protein samples from dorsal striatum used to assess
617 HTT levels by Western blot. Right: Normalized HTT protein levels relative to actin control values. Data
618 are represented as mean ± SEM.

619

620 Figure 2. Neurohistolology of huntingtin knockout in the mouse dorsal striatum. A Representative control
621 and wtHTT cKO slices histologically stained with hematoxylin and eosin (H&E) Scale bar: 30 µm. B
622 Representative control and wtHTT cKO slices histologically stained with cresyl violet. Scale bar: 30 µm.
623 C Left: Representative images of Golgi-stained dendrites from control and wtHTT cKO striatal slices.
624 Scale bar: 2 µm. Right: Individual data and average spine density, number of thin, stubby and mushroom
625 spines from 10 µm dendritic segments. D Left: Representative images of control and wtHTT cKO slices
626 immunostained with DAPI. Right: Analysis of nuclear density. Scale bar: 50 µm. Data are represented as
627 mean ± SEM.

628

629 Figure 3. Huntingtin knockout results in astrocyte gliosis in the dorsal striatum. A Representative images
630 of control and wtHTT cKO slices immunohistochemically stained for glia analysis. Scale bar: 50 µm. B
631 Average GFAP staining. C Percentage of FOV with GFAP positive signal. D IBA-1 staining intensity. E
632 Percentage of FOV with IBA-1 positive signal. Data are represented as mean ± SEM.

633

634 Figure 4. Deletion of huntingtin reduces intrinsic excitability in the mouse striatum. A Representative IV
635 traces of control and wtHTT cKO neurons. B Current-voltage curve showing average number of APs

636 generated at each current sweep. C Average rheobase. D Average AP threshold. E Average RMP. F
637 Average membrane resistance. G Average membrane capacitance. H Representative sEPSC traces of
638 control and wtHTT cKO neurons (axes: x pA, y second). I Average sEPSC frequency. J Average IEI. K
639 Average sEPSC amplitude. Data are represented as mean ± SEM.
640
641 Figure 5. Huntingtin conditional knockout in the mouse striatum does not influence general motor activity
642 or motor learning. OFT A Representative traces of ANYmaze video tracked movements of control and
643 wtHTT cKO mice. B Left: Average total distance travelled. Right: Average speed. Accelerated rotarod C
644 Average latency to fall on rotarod.
645
646 Figure S1. A OFT data separated by sex. B Rotarod data separated by sex. Data were assessed for sex
647 differences by two-way repeated measures ANOVA (B) and two-way ANOVA and are represented as
648 mean ± SEM.
649
650
651
652
653
654
655
656
657
658

659 **Tables**

660 Table 1 Statistical tests used and accompanying values.

661

Figure #	*Experiment*	*Animal (N) and cell/image/slice number (n)*	*Statistics performed*	*p value*	*Degrees of freedom/ F (DFn, DFd)*
1C	HTT western blot	N=4, hemisphere n = 8	Unpaired parametric t test	CTL vs cKO: p = 0.0061	1.646 (6, 5)
2C	Spine density	N = 4, hemisphere n = 4, dendrite n = 26	Unpaired parametric t test	CTL vs cKO: p = 0.4583	(1.122) 25, 25
2C	Number of thin spines	N = 4, hemisphere n = 4, dendrite n = 26	Mann-Whitney test	CTL vs cKO: p = 0.1859	Not reported
2C	Number of stubby spines	N = 4, hemisphere n = 4, dendrite n = 26	Mann-Whitney test	CTL vs cKO: p = 0.6129	Not reported
2C	Number of mushroom spines	N = 4, hemisphere n = 4, dendrite n = 26	Mann-Whitney test	CTL vs cKO: p = 0.3819	Not reported
2D	DAPI nuclear density	N=4, hemisphere n = 8	Unpaired parametric t test	CTL vs cKO: p = 0.0865	(3.444) 15, 14
3B	GFAP intensity	N=4, hemisphere n = 8	Mann-Whitney test	CTL vs cKO: p = 0.0085	Not reported
3B	GFAP % area	N=4, hemisphere n = 8	Mann-Whitney test	CTL vs cKO: p = 0.0750	Not reported
3B	IBA-1 intensity	N=4, hemisphere n = 8	Unpaired parametric t test	CTL vs cKO: p = 0.6575	5.668 (15, 15)
3B	IBA-1 % area	N=4, hemisphere n = 8	Mann-Whitney test	CTL vs cKO: p = 0.2352	Not reported
4B	IV plot	N = 4, cell n = 13-22	Two-way ANOVA Repeated measures (mixed effects)	Genotype (CTL vs cKO): p = 0.0003	Genotype: 16.65 (1, 33)
4C	Rheobase	N = 4, cell n = 13-22	Mann-Whitney test	CTL vs cKO: p = 0.0001	Not reported
4D	Action Potential Threshold	N = 4, cell n = 13-22	Unpaired parametric t test	CTL vs cKO: p = 0.0002	(1.755) 12, 21
4E	Resting membrane potential (RMP)	N = 4, cell n = 13-22	Mann-Whitney test	CTL vs cKO: p = 0.0192	Not reported

4F	Membrane resistance	N = 4, cell n = 13-22	Mann-Whitney test	CTL vs cKO: p = 0.0056	Not reported
4G	Membrane capacitance	N = 4, cell n = 13-19	Outliers excluded, unpaired parametric t test (cleaned data)	CTL vs cKO: p = 0.5264	(6.374) 12, 18
4I	Frequency	N = 4, cell n = 12-19	Mann-Whitney test	CTL vs cKO: p = 0.1770	Not reported
4J	IEI	N = 4, cell n = 12-19	Mann-Whitney test	CTL vs cKO: p = 0.1770	Not reported
4K	Amplitude	N = 4, cell n = 12-19	Mann-Whitney test	CTL vs cKO: p = 0.0585	Not reported
5B	OFT average distance	N = 20	Mann-Whitney test	CTL vs cKO: p = 0.5117	Not reported
5B	OFT average speed	N = 20	Mann-Whitney test	CTL vs cKO: p = 0.5244	Not reported
5C	Accelerating rotarod – latency to fall	N = 20	Two-way ANOVA	Genotype (CTL vs cKO): p =0.8883	0.01999 (1, 38)

662

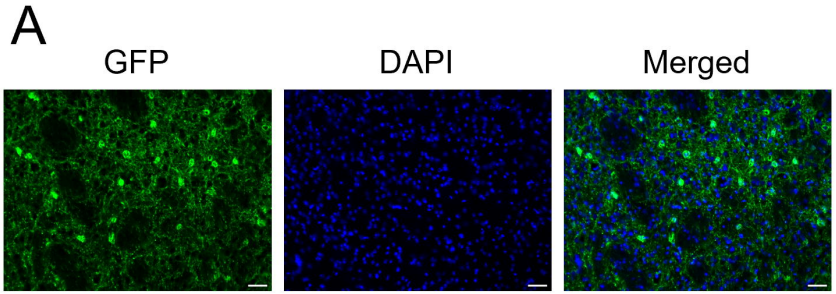
A
GFP
DAPI
Merged

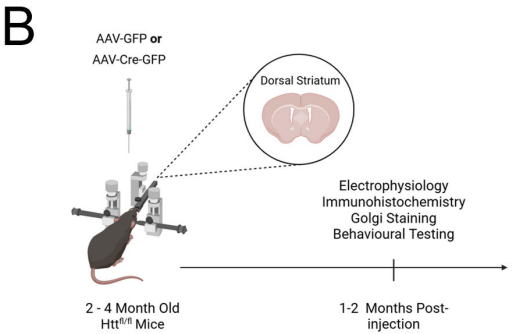
B
AAV-GFP or
AAV-Cre-GFP
Dorsal Striatum
Electrophysiology
Immunohistochemistry
Golgi Staining
Behavioural Testing
2 - 4 Month Old
Htt$^{fl/fl}$ Mice
1-2 Months Post-
injection

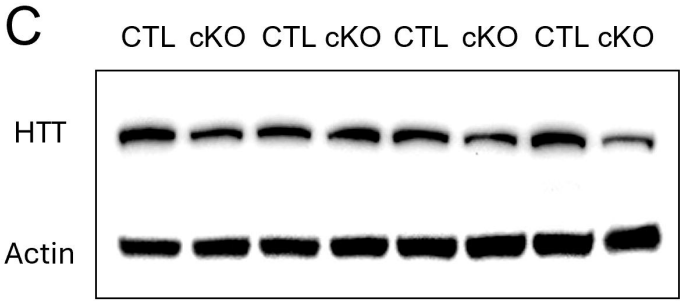
C
CTL cKO CTL cKO CTL cKO CTL cKO
HTT
Actin

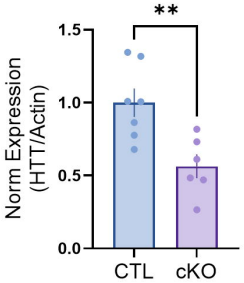
**
1.5
1.0
0.5
0.0
Norm Expression
(HTT/Actin)
CTL
cKO

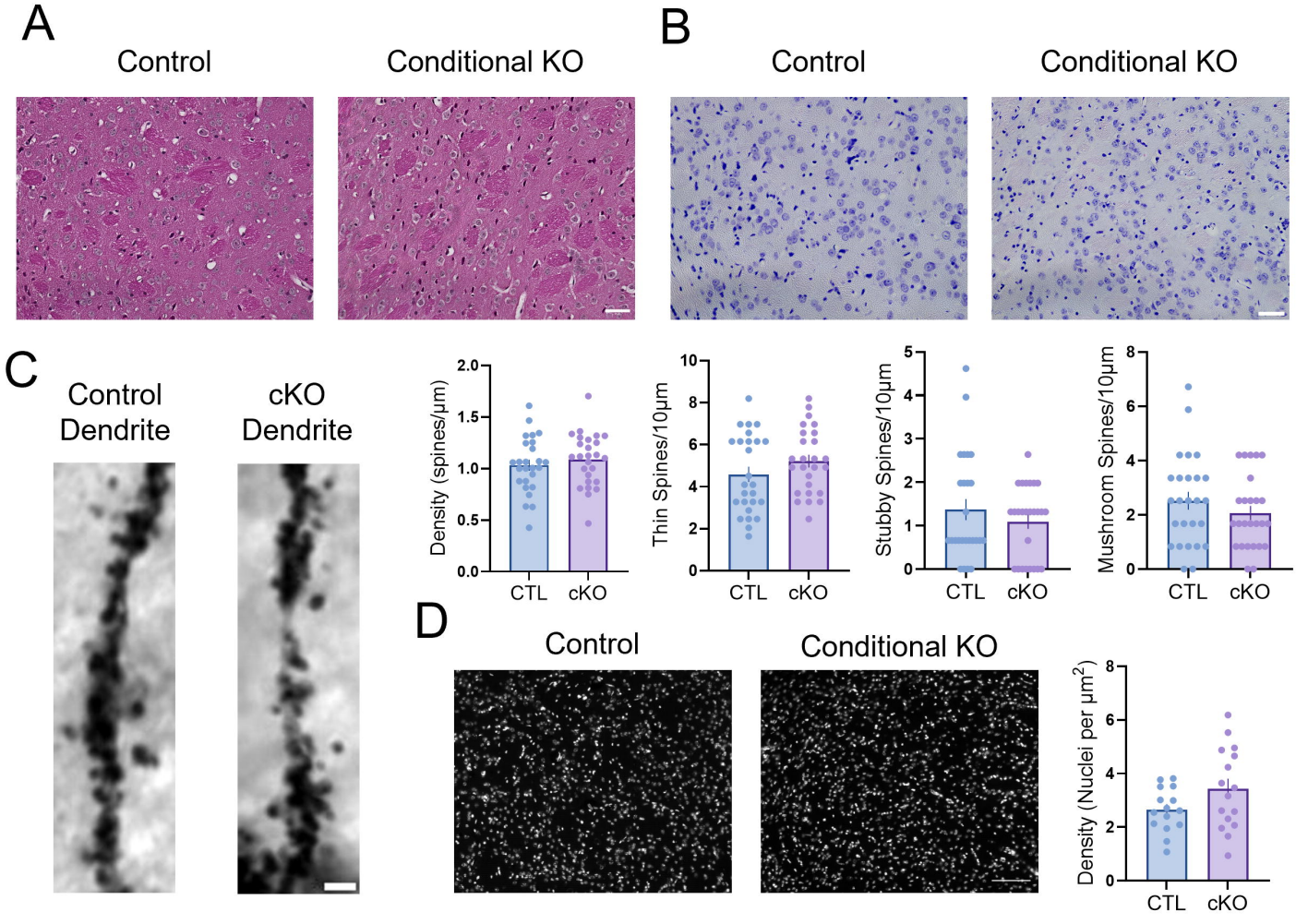
A
Control
Conditional KO
B
Control
Conditional KO
C
Control Dendrite
cKO Dendrite
Density (spines/µm)
2.0
1.5
1.0
0.5
0.0
CTL
cKO
Thin Spines/10µm
10
8
6
4
2
0
CTL
cKO
Stubby Spines/10µm
5
4
3
2
1
0
CTL
cKO
Mushroom Spines/10µm
8
6
4
2
0
CTL
cKO
D
Control
Conditional KO
Density (Nuclei per µm2)
8
6
4
2
0
CTL
cKO

A

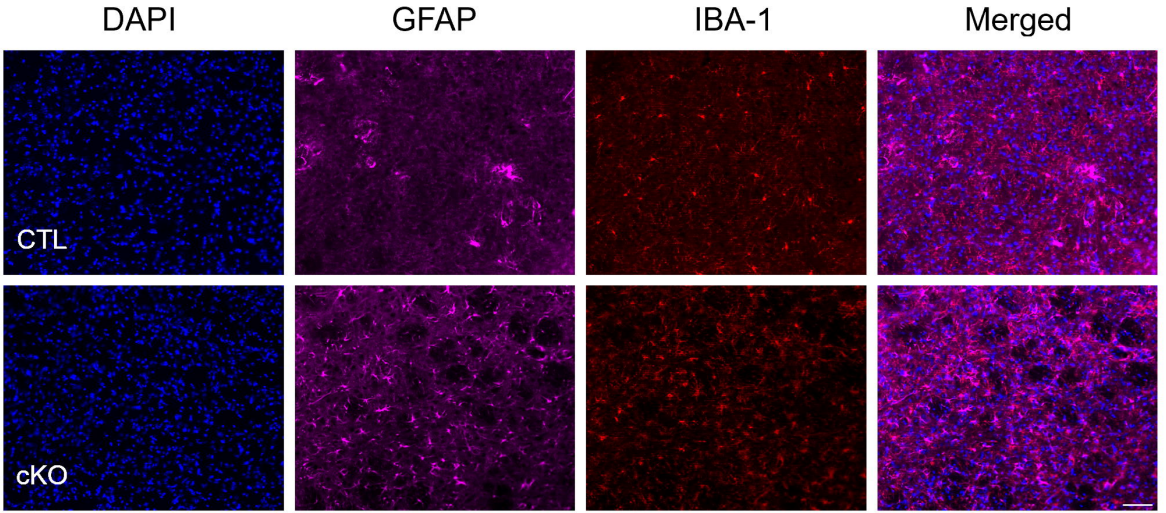
DAPI
GFAP
IBA-1
Merged
CTL
cKO

B

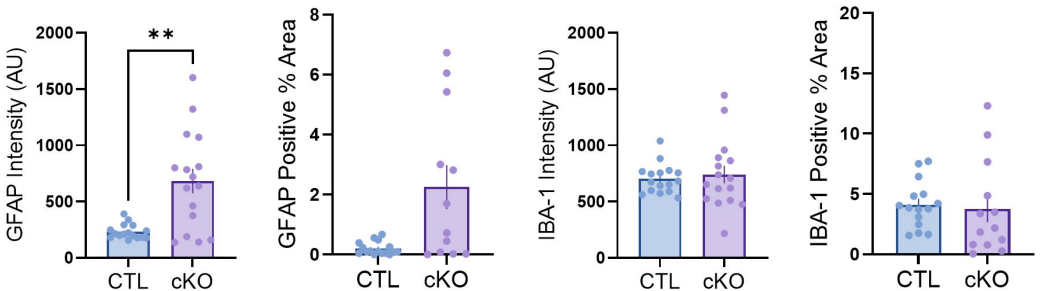
GFAP Intensity (AU)
2000
1500
1000
500
0
**
CTL
cKO
GFAP Positive % Area
8
6
4
2
0
CTL
cKO
IBA-1 Intensity (AU)
2000
1500
1000
500
0
CTL
cKO
IBA-1 Positive % Area
20
15
10
5
0
CTL
cKO

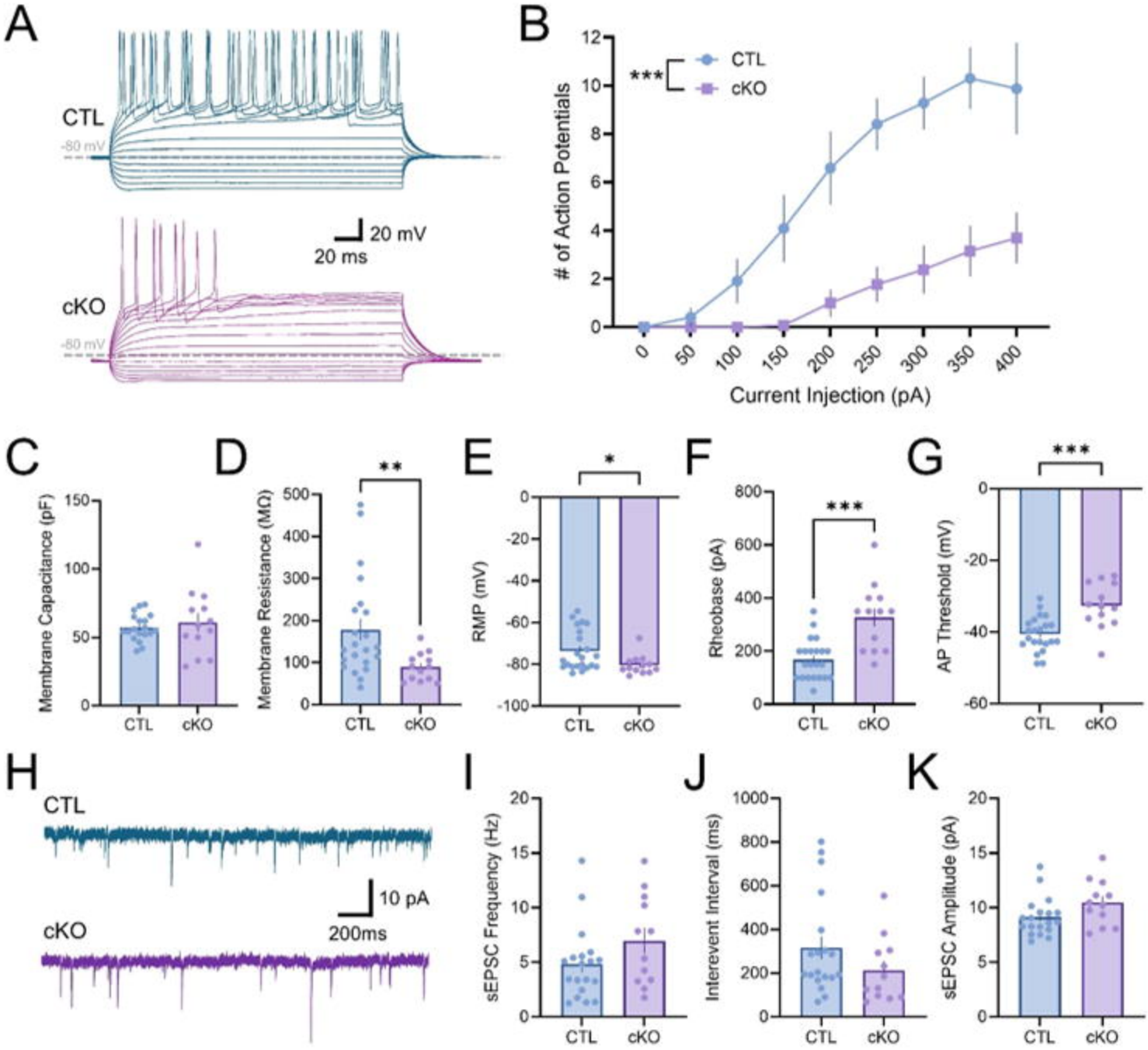
A
CTL
-80 mV
20 mV
20 ms
cKO
-80 mV
B
***
CTL
cKO
# of Action Potentials
Current Injection (pA)
C
Membrane Capacitance (pF)
CTL
cKO
D
**
Membrane Resistance (MΩ)
CTL
cKO
E
*
RMP (mV)
CTL
cKO
F
***
Rheobase (pA)
CTL
cKO
G
***
AP Threshold (mV)
CTL
cKO
H
CTL
10 pA
200ms
cKO
I
sEPSC Frequency (Hz)
CTL
cKO
J
Interevent Interval (ms)
CTL
cKO
K
sEPSC Amplitude (pA)
CTL
cKO

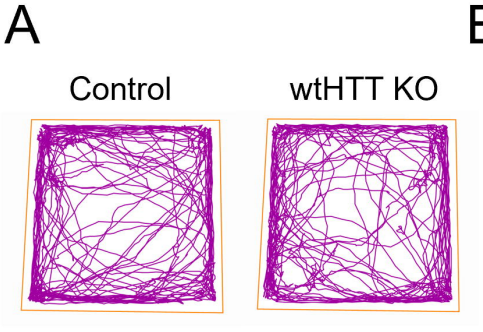

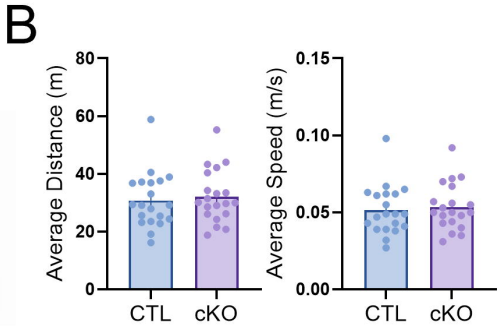

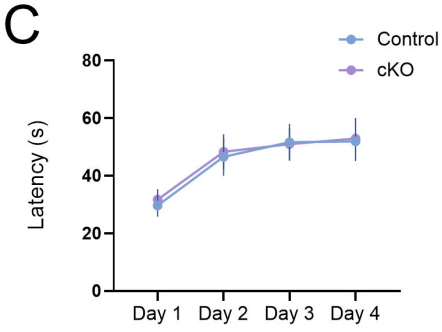

Open Field Test

Accelerating Rotarod

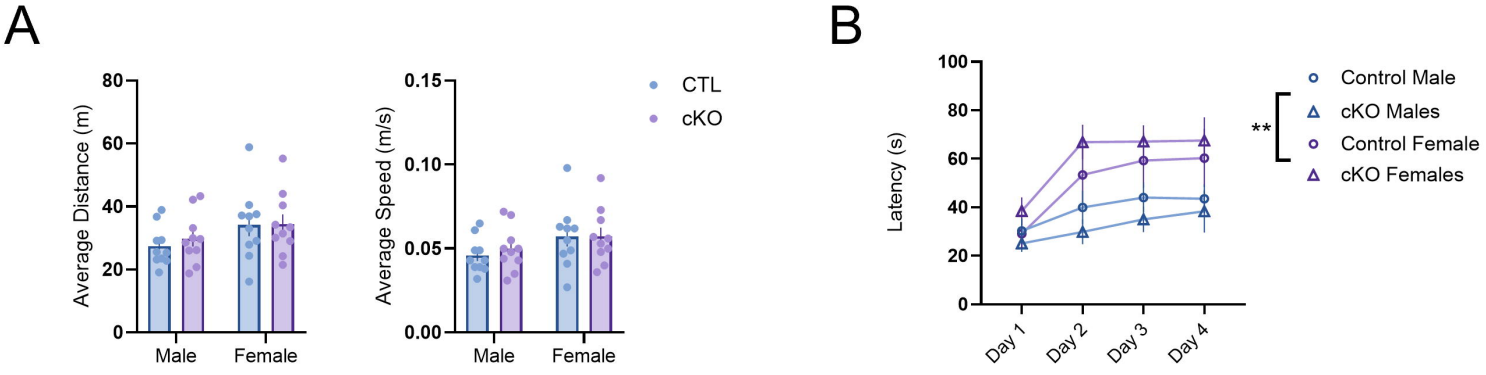
A
Average Distance (m)
80
60
40
20
0
Male
Female
Average Speed (m/s)
0.15
0.10
0.05
0.00
Male
Female
CTL
cKO
B
Latency (s)
100
80
60
40
20
0
Day 1
Day 2
Day 3
Day 4
**
Control Male
cKO Males
Control Female
cKO Females